Author Manuscript

Author Manuscript

Author Manuscript

Author Manuscript

HHS Public Access

Author manuscript

Neuron. Author manuscript; available in PMC 2025 May 01.

Published in final edited form as:

Neuron. 2024 May 01; 112(9): 1416–1425.e5. doi:10.1016/j.neuron.2024.02.002.

Transient cAMP production drives rapid and sustained spiking in brainstem parabrachial neurons to suppress feeding

Jonnathan Singh Alvarado[1,†], **Andrew Lutas**[1,2,†,*], **Joseph C. Madara**[1], **Jeremiah Isaac**[2], **Caroline Lommer**[1], **Crystian Massengill**[3], **Mark L. Andermann**[1,*]

[1]Division of Endocrinology, Metabolism, and Diabetes, Beth Israel Deaconess Medical Center, Harvard Medical School, Boston, MA 02115 USA

[2]Diabetes, Endocrinology, and Obesity Branch, National Institutes of Diabetes and Digestive and Kidney Diseases, National Institutes of Health, Bethesda, MD 20892 USA

[3]Program in Neuroscience, Harvard Medical School Boston, MA 02115 USA

Summary

Brief stimuli can trigger longer lasting brain states. G protein-coupled receptors (GPCRs) could help sustain such states by coupling slow-timescale molecular signals to neuronal excitability. Brainstem parabrachial nucleus glutamatergic neurons (PBN^{Glut}) regulate sustained brain states such as pain, and express Gs-coupled GPCRs that increase cAMP signaling. We asked whether cAMP in PBN^{Glut} neurons directly influences their excitability and effects on behavior. Both brief tail shocks and brief optogenetic stimulation of cAMP production in PBN^{Glut} neurons drove minutes-long suppression of feeding. This suppression matched the duration of prolonged elevations in cAMP, Protein Kinase A (PKA) activity, and calcium activity *in vivo* and *ex vivo*, as well as sustained, PKA-dependent increases in action potential firing *ex vivo.* Shortening this elevation in cAMP reduced the duration of feeding suppression following tail shocks. Thus, molecular signaling in PBN^{Glut} neurons helps prolong neural activity and behavioral states evoked by brief, salient bodily stimuli.

eTOC blurb

Singh Alvarado, Lutas and colleagues used optical tools to demonstrate that persistent cAMP signaling directly couples to neuronal activity in the parabrachial nucleus to drive sustained suppression of feeding. The results suggest that cAMP produced by transient GPCR activation can extend the timescale of neuronal activity from seconds to minutes.

[*]Correspondence: Andrew Lutas, andrew.lutas@nih.gov, Mark Andermann, manderma@bidmc.harvard.edu.
[†]Contributed equally to this study.
Lead contact: Mark Andermann, Mark Andermann, manderma@bidmc.harvard.edu

Author Contributions

Conceptualization, J.S.A., A.L. and M.L.A.; investigation, A.L, J.S.A., J.M., J.I., C.I.M., and C.L.; formal analysis & visualization, J.S.A., A.L. and M.L.A.; writing – original draft, J.S.A. and A.L., writing – review & editing, J.S.A., A.L., and M.L.A.

Declaration of Interests

The authors declare no competing interests.

Publisher's Disclaimer: This is a PDF file of an unedited manuscript that has been accepted for publication. As a service to our customers we are providing this early version of the manuscript. The manuscript will undergo copyediting, typesetting, and review of the resulting proof before it is published in its final form. Please note that during the production process errors may be discovered which could affect the content, and all legal disclaimers that apply to the journal pertain.

Author Manuscript Author Manuscript Author Manuscript Author Manuscript

Introduction

Behavioral states such as nausea, pain and associated arousal persist for minutes to hours. Such states are likely driven by slow-timescale changes in neural activity, yet it is not clear how these persistent shifts in activity occur. One possibility involves the sustained elevation in cyclic AMP (cAMP) production driven by G_s-coupled GPCRs. However, determining whether and how cAMP changes in any brain region control the duration of behavioral states has been challenging, due in part to technical limitations in studying cAMP signaling. Recent advances have enabled the study of cAMP signaling in awake animals[1–5]. For example, G_s-coupled GPCRs can convert brief neurotransmitter release in the hypothalamus into hours-long persistent behavioral states, such as elevated mating drive, that match the duration of cAMP signaling[3]. However, depending on the set of regulators and downstream targets of cAMP signaling in a given cell type and brain area, cAMP signaling may persist for hours[3] or only for seconds[2,6], and may not couple to neural excitability[2,7].

We focused on the parabrachial nucleus (PBN), a brainstem region where neurons express many GPCRs that drive or suppress cAMP production[8–10]. We used new tools to track and manipulate cAMP in PBN^{Glut} neurons. As the PBN is a key node in the control of ingestive, nausea, and pain-related behaviors[11–21], we investigated how cAMP signaling influences the duration of pain-evoked suppression of feeding, a PBN-dependent behavior[22–24]. Pain-evoked suppression of feeding lasted for tens of seconds, depended on sustained cAMP signaling, and could be mimicked by brief, light-evoked elevations in cAMP in PBN^{Glut} neurons. Using *in vivo* and *ex vivo* optical and electrophysiological approaches, we discovered that cAMP rapidly controls PBN^{Glut} neuron excitability. Thus, cAMP signaling provides a mechanism for translating various neuropeptidergic, hormonal and other signals acting on different PBN^{Glut} neurons into sustained neural activity and behavior, with additional specificity conferred by selective expression of GPCRs and phosphodiesterases that regulate the levels and dynamics of cAMP in different PBN^{Glut} neuron types[9,10].

Results

Brief salient events can halt feeding for extended periods of time

We focused on a behavior that demonstrated sustained suppression following a brief, salient stimulus: shock-induced suppression of continuous feeding. We used head-fixation to allow precise delivery of the same salient stimulus while measuring food consumption in combination with optical stimulation and cellular recordings (Figure 1A). Food-restricted mice were acclimated to head restraint and trained to associate licking at a lickspout with the delivery of a palatable liquid food, Ensure (Figure 1B). Mice licked at a steady rate, but stopped licking for an extended period (~30–60 seconds) following a 10-s tail shock stimulus (Figure 1B,C). Thus, despite a high motivation to consume food, the tail shock stimulus resulted in motivational suppression that outlasted the stimulus.

cAMP-dependent signaling in PBN^{Glut} neurons controls prolonged suppression of feeding

We next asked whether second messenger signaling in PBN^{Glut} neurons might underlie this extended suppression of feeding. Many subtypes of PBN^{Glut} neurons together play key roles

Author Manuscript Author Manuscript Author Manuscript Author Manuscript

in pain responses including the suppression of feeding[11,12,14–16,25,26]. Neuromodulators that signal through G_s-coupled GPCRs, which promote production of cAMP and activation of its main effector, protein kinase A (PKA), suppress feeding through their effects on PBN[25,27]. Thus, we asked whether PBN^{Glut} neurons exhibited prolonged PKA signaling driven by this transient tail shock (Figure 1D).

We took advantage of a genetically-encoded fluorescent reporter of PKA activity[2,3,28] (ExRai-AKAR2), which we previously found to be sensitive enough to detect tail shock-evoked PKA signaling[2]. We expressed ExRai-AKAR2 in PBN^{Glut} neurons and performed fiber photometry during shock-evoked feeding suppression (Figure 1D, Supplemental Figure 2A). We found that tail shock evoked an increase in PKA activity that peaked following shock offset and lasted for tens of seconds (Figure 1E). The evoked PKA signal was of variable amplitude but consistent duration across trials (Figure 1F). Accordingly, shock-evoked PKA activity correlated with the duration of lick suppression ($R = 0.82$; $p = 0.001$), but not the duration of locomotion ($R = 0.38$; $p = 0.22$; Figure 1F). These results suggest that the strength and dynamics of cAMP-dependent signaling in PBN^{Glut} neurons may control PBN^{Glut} neuronal activity to arrest ongoing motivated behavior.

To directly test whether elevation of cAMP in PBN^{Glut} neurons determines the duration of this behavioral suppression, we expressed a constitutively active phosphodiesterase, which rapidly degrades cAMP, unilaterally in PBN^{Glut} neurons (Figure 1G; PDE4D3-Cat[2,3]). As in previous work[2,3,29], PDE4D3-expression did not lead to cell death (Supplemental Figure 1A,B), and PDE4D3-expressing neurons fired fewer action potentials than control neurons in response to current injection *ex vivo* (Supplemental Figure 1C-E), suggesting that basal levels of cAMP regulate excitability of PBN^{Glut} neurons. PDE4D3-expressing mice exhibited significantly shorter periods of feeding suppression, despite displaying a similar locomotor response to tail shock (Figure 1H,I). Thus, cAMP accumulation in PBN^{Glut} neurons is necessary for the prolonged pause in feeding following tail shock.

Transient photostimulated production of cAMP suppresses food seeking for tens of seconds

Given the necessity of cAMP in setting the duration of feeding suppression following tail shock, we asked whether we could mimic this suppression by directly increasing cAMP in PBN^{Glut} neurons, bypassing the transient activation of G_s-GPCRs by diverse neuromodulators and peptides (Figure 2A,B). We expressed a blue-light activated adenylyl cyclase (biPAC[2,3]) bilaterally in PBN^{Glut} neurons to photostimulate cAMP production (Figure 2B, Supplemental Figure 2B). Photostimulation using low-intensity blue light (1 mW; five 1-s pulses every 2 s; Figure 2B) robustly suppressed ongoing food seeking and consumption for tens of seconds (Figure 2C,D) for a similar duration as tail shock (Figure 1C).

We next asked whether photostimulation of cAMP would also reduce home cage consumption of chow following a 24 hour fast. After allowing mice to consume food for 30 minutes, we bilaterally photostimulated cAMP production during the remaining 90 minutes of access to food using a low intensity stimulation paradigm (100 ms every 10 s; ~1 mW) that should maintain continuously elevated cAMP levels in PBN^{Glut} neurons (Figure 2E

Author Manuscript Author Manuscript Author Manuscript Author Manuscript

and Figure 3). We observed an almost complete absence of food consumption during this period (Figure 2F). Mice resumed normal feeding rates a few minutes following cessation of photostimulation, even when using higher-intensity photostimulation (~5 mW; Figure 2G). We also examined other effects of photostimulation protocols used throughout this study, and found that they all had similar effects on feeding suppression, while the stronger stimulation protocols also evoked significant suppression of locomotion (Supplemental Figure 1F,G).

Finally, to assess whether mice found this photostimulation to be aversive, we used a real-time place aversion assay (RTPA; Supplemental Figure 1H-L). Across three sessions, mice avoided the side paired with photostimulation and were less mobile on the unstimulated side (Supplemental Figure 1H-J). Mice also developed a learned avoidance of the paired side during an initial exploratory period without photostimulation (Supplemental Figure 1K,L).

Photostimulated production of cAMP persists for tens of seconds in some PBN^{Glut} neurons

We next assessed the dynamics by which cAMP decays to baseline following photostimulation. We co-expressed the fluorescent cAMP biosensor cADDis[1–3] together with biPAC in PBN^{Glut} neurons, implanted a gradient index (GRIN) lens in lateral PBN, and performed two-photon imaging in awake mice (Figure 3A, Supplemental Figure 2C). Brief photostimulation of cAMP (100 ms, as in Figure 2E) evoked robust increases in cAMP in all PBN^{Glut} neurons that expressed both biPAC and cADDis (Figure 3B). Following photostimulation, the elevation in cAMP persisted for tens of seconds before decaying to baseline (median τ, 33.2 seconds). In contrast to the slower dynamics observed in the medial preoptic nucleus of the hypothalamus[3], these rapid decay dynamics[2] indicate that PBN^{Glut} neurons contain abundant levels of endogenous phosphodiesterases that break down cAMP.

Our GRIN lens imaging was restricted to a small subregion of PBN (effective FOV: ~250 μm^2). Thus, we repeated the photostimulation protocol in coronal brain slices, which enabled simultaneous imaging of hundreds of neurons throughout medial and lateral PBN (Figure 3C). We found that all imaged PBN neurons showed sustained elevations in cAMP following biPAC photostimulation. Given the diversity and spatial organization of cell types in the PBN[9,10], we characterized the decay dynamics across PBN neurons in all FOVs (Supplemental Figure 3A). The decay time constants of cAMP clearance were highly variable (10s to 100s of seconds) between individual neurons both within and across brain slices, but were not systematically different across the major subdivisions of PBN (Supplemental Figure 3B,C).

Photostimulation of cAMP drives persistent increases in calcium activity in some PBN^{Glut} neurons

Given the correspondence between feeding suppression and elevated cAMP levels in PBN^{Glut} neurons, we hypothesized that increases in cAMP lead to immediate and sustained increases in neuronal activity in at least some PBN^{Glut} neurons. We test this prediction using *in vivo* imaging of PBN^{Glut} neurons co-expressing biPAC and the calcium sensor GCaMP6s. We focused on neurons with confirmed biPAC expression and rapid GCaMP6s fluctuations

Author Manuscript Author Manuscript Author Manuscript Author Manuscript

(Figure 4A, Supplemental Figure 2D). Photostimulated cAMP production evoked GCaMP6s fluorescence transients in 34.5% (24/71) of these PBN^{Glut} neurons, suggesting that some but not all neurons can translate cAMP into neuronal activity (Figure 4B). Notably, these GCaMP6s responses to the 100 ms light pulse could last for several tens of seconds. BiPAC expression levels were not correlated with the magnitude of light-evoked GCaMP6s activity (Supplemental Figure 3D,E).

To study the mechanism(s) underlying this cAMP-driven PBN^{Glut} neuron activity, we turned to acute brain slices. Upon photostimulation, ~34% of neurons (1437/4264) displayed a rapid increase in GCaMP6s fluorescence, similar to the proportion observed *in vivo* (Figure 4C-D). The duration of GCaMP6s responses tended to be longer in the dorsomedial vs. ventrolateral subregion of lateral PBN (Supplemental Figure 3F, G), despite a lack of systematic spatial differences in the duration of evoked cAMP responses across these regions (Supplemental Figure 3A-C).

These findings indicate that PBN^{Glut} neurons show prolonged elevations in cAMP following biPAC stimulation, and a subset also show increased calcium activity. To confirm that these cAMP-dependent increases in activity were not simply due to our biPAC protocol, we applied the adenylyl cyclase activator forskolin to elevate cAMP while simultaneously recording both the green cAMP sensor, cADDis, and the red calcium indicator, jRGECO. Consistent with our findings using biPAC, the majority of PBN^{Glut} neurons expressing cADDis (~92%) showed increased cAMP upon forskolin application, while less than half of these neurons (~44%) showed a subsequent increase in calcium activity (Supplemental Figure 3H-J).

cAMP drives spiking in PBN^{Glut} neurons

We confirmed that the increases in GCaMP6s fluorescence following brief biPAC stimulation of cAMP reflected sustained increases in spiking activity of PBN^{Glut} neurons, as they were largely absent when we blocked neuronal spiking using tetrodotoxin (TTX, Supplemental Figure 4A). To further assess the magnitude and dynamics of this increase in spiking, we performed cell-attached electrophysiological recordings of PBN^{Glut} neurons expressing biPAC in brain slices. Transient photostimulation of cAMP increased the firing rate, which peaked ~5 seconds after stimulation and slowly decayed to baseline (Figure 4E,F), approximately matching the time course of our *ex vivo* GCaMP6s imaging experiments.

A key finding in Figure 1 was that the duration of tail-shock-evoked feeding suppression was blunted by expression of a constitutively active phosphodiesterase, PDE4D3-Cat. To confirm that PDE4D3-Cat expression curtails the duration of increases in firing rate, we performed cell-attached recordings in PBN^{Glut} neurons from mice that expressed biPAC bilaterally, or that expressed biPAC bilaterally and PDE4D3-Cat unilaterally (Figure 4E). In comparison to PBN^{Glut} neurons expressing biPAC only, those co-expressing biPAC and PDE4D3-Cat showed weaker photostimulation-evoked increases in firing rate that decayed more quickly to baseline (Figure 4F, G).

Author Manuscript Author Manuscript Author Manuscript Author Manuscript

PKA activity contributes to the coupling between cAMP and neuronal activity

To understand how cAMP drives neuronal activity, we performed a series of pharmacology experiments using our GCaMP6s slice imaging preparation. To test whether cAMP increased neural activity via increased ionotropic glutamate receptor synaptic transmission, we stimulated biPAC in the presence of AMPA and NMDA receptor antagonists, CNQX and D-APV. Blocking excitatory transmission in this way resulted in a modest but significant reduction in biPAC-evoked activity (−19.2% relative to control, Figure 4H and Supplemental Figure 4B), suggesting that local excitatory connectivity partially contributes to the increased activity.

cAMP can influence neuronal activity via downstream effectors such as PKA, as well as via hyperpolarization-activated cyclic nucleotide gated (HCN) channels[30,31]. Application of the HCN channel blocker ZD7288 (ZD) reduced biPAC-evoked activity by 25.5% relative to controls (Supplemental Figure 4C). PKA inhibitors (PKI and H-89) resulted in a larger reduction in biPAC-evoked activity (−38.8% relative to control, Figure 4I, Supplemental Figure 4D). Finally, we tested whether the effects of ZD and PKA inhibitors could be synergistic, while also testing whether cyclic-nucleotide gated channels (CNGs[32]) could play a role in translating cAMP to activity. A cocktail of the HCN blocker ZD, the CNG blocker L-cis-diltiazem, and the PKA inhibitors led to a greater reduction in biPAC-evoked activity (−55.5% relative to control, Supplemental Figure 4E) than when using HCN blockers or PKA inhibitors alone, suggesting that multiple mechanisms link cAMP to neural activity in PBN^{Glut} neurons.

Discussion

In contrast to the more common roles of cAMP as a slow regulator of synaptic plasticity, development, and learning[6,33], our findings demonstrate a more direct role for cAMP in increasing neuronal spiking in the PBN. Specifically, in response to brief, salient bodily signals, elevations in cAMP in PBN^{Glut} neurons can drive extended neuronal activation and suppression of feeding.

Endogenous neuromodulatory and peptidergic modulators of cAMP in PBN neurons

Our photometry experiments were designed to investigate the contribution of prolonged cAMP signaling to the sustained behavioral response to a tail shock. While it remains unknown precisely which endogenous ligands and receptors drive the relevant cAMP/PKA signaling in PBN neurons, several candidates exist. For example, noradrenergic neurons in the locus coeruleus and nucleus of the solitary tract release noradrenaline in response to noxious stimuli and drive long-lasting potentiation of PBN neurons[22,25,34]. Painful stimuli also activate spinal inputs to PBN that express the neuropeptide substance P[16,35,36], which in turn activates PBN neurons that express the G_s-coupled receptor for substance P, Tacr1[37]. Dopaminergic neurons in the ventral tegmental area could also increase cAMP levels via activation of Drd1 receptors in PBN[27].

More broadly, single-cell sequencing studies have identified unique patterns of GPCR expression across PBN cell types[9,10], suggesting that release of a given ligand could drive

Author Manuscript Author Manuscript Author Manuscript Author Manuscript

cAMP changes in specific PBN subtypes. For example, neuropeptide-Y (NPY), which via NPY1/2R leads to decreased cAMP, has been demonstrated to counter the ability of inflammatory pain to suppress feeding[17]. Similarly, the mu opioid receptor is highly expressed in the PBN and regulates breathing, arousal and pain sensitivity[38].

Determinants of the duration of cAMP signaling in PBN

Recent work has revealed that neuromodulator release can be integrated over long periods of time (minutes to hours) via cAMP. For example, dopamine released onto medial preoptic area neurons in male mice upon a brief encounter with a female drives hour-long increases in cAMP that, in turn, causes persistent priming of mating behaviors[3]. Related work in flies shows that cAMP signaling through PKA serves as a persistent biochemical signal even in the absence of continuous synaptic input, allowing for cell-autonomous persistent activity[7]. Our findings suggest that similar processes might take place in the PBN in response to a wide variety of acute "threats"[15,39] (e.g., pain, noxious temperatures, toxin consumption) in order to trigger defensive behavioral responses that can persist beyond the duration of the initial threat stimulus[14,39].

The duration of elevated cAMP and its effects on spiking and behavior may be modifiable via regulation of endogenous phosphodiesterase activity in PBN^{Glut} neurons. Indeed, we queried two recent single-cell sequencing datasets[9,10], and found that several phosphodiesterases (PDE1a, PDE10a, PDE7b, PDE8b) are expressed in specific subtypes of PBN neurons, while others (PDE4b, PDE4d) are highly expressed throughout all PBN subtypes. Further, PDE1a is activated by calcium[40], indicating an additional negative-feedback mechanism by which neural activity may shorten the duration of future elevations in cAMP.

Coupling of cAMP to spiking

While most PBN^{Glut} neurons had the capacity for sustained cAMP signaling across tens of seconds to minutes, photostimulation of cAMP production drove spiking of spiking-related calcium activity in less than half of PBN^{Glut} neurons. What determines which neurons ultimately translate cAMP into neural activity? One possibility is that differential expression of PKA determines each neuron's response, possibly via PKA-dependent phosphorylation of ion channels that are differentially expressed across subtypes of PBN^{Glut} neurons[9,10]. Moreover, most subunits of PKA appear highly expressed throughout the PBN (Allen Brain Atlas), but distinct isoforms appear biased towards PBN subregions. This differential expression could account for the spatial gradient we observed, where activity driven by cAMP is more sustained in the dorsomedial region of lateral PBN. Because different subtypes of PBN^{Glut} neurons are concentrated in distinct subregions of PBN[9,10], we considered whether various candidate ion channels[12,19] involved in converting cAMP elevations to spiking were enriched in specific molecularly-defined PBN neuron subtypes. While we did not observe specific clustering of ion channels in individual cell types, some channels showed variable expression across neurons (not shown), which could contribute to the variability in coupling of cAMP to spiking across neurons. Finally, we did not test the contribution of other mechanisms such as direct coupling to ion channels and to exchange proteins directly activated by cAMP (EPAC), both of which can depolarize neurons[32,41,42].

Author Manuscript Author Manuscript Author Manuscript Author Manuscript

Thus, future work could more precisely define the mechanism(s) by which cAMP regulates neuronal excitability in PBN.

Potential limitations of this study

We investigated effects of cAMP in an unbiased manner by considering all glutamatergic neurons in PBN. Further studies are needed to confirm that the subset of PBN^{Glut} neurons in which cAMP couples to spiking indeed contains the neurons driven by tail shock, and to investigate how cAMP influences the activity of distinct PBN^{Glut} subtypes that regulate respiration[38,43,44], malaise-induce anorexia[11,14,45,46], thermoregulation[47,48], feeding[27,49–53], and pain sensitization[12,19,21,37,54–56]. Further, our ability to monitor cAMP dynamics during natural behaviors was hampered by the sensitivity of the cADDis sensor *in vivo*, which motivated us to use other sensors such as ExRai-AKAR2 to track PKA activity as a proxy for cAMP. Newly emerging tools may allow for more sensitive interrogation of cAMP signaling[28,57,58] in more naturalistic conditions.

STAR Methods

Resource Availability

Lead Contact: Further information and requests for resources and reagents should be directed to and will be fulfilled by the lead contact, Mark Andermann (manderma@bidmc.harvard.edu).

Materials Availability: For inquiries regarding the cADDis plasmid and virus generated during this study, please contact Montana Molecular. Plasmids for mKate2-biPAC and mKate2-PDE4D3-cat were previously generated (Zhang et al., 2021) and deposited to Addgene [catalog # 169127 & 169128].

Data and Code Availability: Data reported in this paper will be shared by the lead contact upon request. This paper does not report original code. Any additional information required to reanalyze the data reported in this paper is available from the lead contact upon request.

EXPERIMENTAL MODEL AND SUBJECT DETAILS

All animal care and experimental procedures were approved by the Beth Israel Deaconess Medical Center Institutional Animal Care and Use Committee. Animals were singly housed on a 12-h light/dark cycle with standard mouse chow and water provided ad libitum unless they were used for feeding-related experiments, in which case they were food restricted (~2.5 g of standard chow per day for a maximum of 2 weeks, with daily weight monitoring) to maintain body weight at 10 – 15% of free-feeding weight. All experiments were performed on adult Vglut2-ires-cre mice (Jackson Lab Strain # 016963; 29 male and 17 female mice in total) between the ages of 8 and 20 weeks.

METHOD DETAILS

Stereotaxic surgeries—Injections (~150 nl total) were targeted to the ventral edge of PBN (AP: −5.05 mm; DV: −3.8 to −3.7 mm; ML: ± 1.5 mm) to allow for spread of virus via

Author Manuscript Author Manuscript Author Manuscript Author Manuscript

efflux. For experiments with simultaneous biPAC stimulation and cADDis recordings, we injected a 1:1 mixture of AAV1-hSyn-DIO-GreenDownward-cADDis (Boston Children's Hospital Vector Core) and AAV1-EF1a-DIO-mKate2-biPAC (Boston Children's Hospital Vector Core). For cell-attached experiments, we injected a 1:1 mixture of AAV1-EF1a-DIO-Venus-biPAC and AAV1-EF1a-DIO-mKate2-PDE4D3-cat (Boston Children's Hospital Vector Core), or a 1:1 mixture of AAV1-EF1a-DIO-Venus-biPAC and phosphate buffered saline. For optogenetic stimulation experiments, we used AAV1-EF1a-DIO-mKate2-biPAC followed by implantation of optic fibers. For photometry recordings of PKA activity, we injected AAV2/9.hSyn.FLEX.ExRai-AKAR2-CW3SL (gift from Huganir lab) followed by implantation of optic fibers. For experiments testing the role of cAMP signaling on feeding behavior, we either injected mice with AAV1-EF1a-DIO-mKate2-biPAC or AAV1-EF1a-DIO-mKate2-PDE4D3-cat.

Fiber photometry recording—Optic fibers with a metal ferrule (400 μm diameter core; multimode; numerical aperture (NA) 0.48; 5.0 mm length; Doric Fibers; MFC_400/430–0.48_5mm_MF1.25_FLT) were bilaterally implanted over PBN (Bregma: AP: −5.05 mm; DV: −3.65 mm; ML: ±1.5 mm). The fibers and a custom-made titanium headpost (H.E. Parmer) were fixed to the skull using C&B Metabond (Parkell). Mice were given at least 2 weeks to recover before any behavioral experiments began. Fiber photometry recordings were performed using head-fixed mice that were free to run on a 3D printed circular treadmill. Fiber optic cables (1 m long; 400 μm core; 0.48 NA; low autofluorescence; Doric Lenses) were coupled to implanted optic fibers with zirconia sleeves (Precision Fiber Products). Black heat shrink material was placed around the fiber coupling to prevent light leakage from interfering with recordings or behavior. Excitation and emission light was passed through a GFP fluorescence minicube (FMC3_E(460–490) F(500–550); Doric Lenses). Excitation light (~100 μW) was provided by a 465 nm LED (Plexon LED and driver) which was modulated at either 217 or 319 Hz using transistor–transistor logic (TTL) output from two lock-in amplifiers (SR830; Stanford Instruments). Emission light was collected by a femtowatt photoreceiver (Newport 2151), demodulated using a lock-in amplifier (SR830; Stanford Instruments) and digitized at 1 kHz sampling rate (PCIe-6321; National Instruments). Data acquisition was controlled using a custom script in MATLAB (MathWorks).

GRIN lens implantation and related surgical procedures—For PBN cell body imaging, immediately after viral injections, mice were implanted with a gradient index (GRIN) lens. We used singlet GRIN lenses (3 mice, GRINtech, NEM-050–25–10–860-S-1.5p; 0.5 mm diameter; 6.5 mm length; 250 μm focal distance on brain side at 860 nm (NA 0.5); 100 μm focal distance on air side (NA 0.5); non-coated) and doublet GRIN lenses (5 mice, GRINtech, NEM-050–25-10–860-DM; 0.5 mm diameter; 9.89 mm length; 250 μm focal distance on brain side at 860 nm (NA 0.47); 100 μm focal distance on air side (NA 0.19)). GRIN lens implantations were performed as previously described[59]. Briefly, mice were maintained under anesthesia (1.5–2.0% isoflurane) and body temperature was maintained using a heating pad in a stereotaxic apparatus (Kopf Instruments, Model 940). A beveled 25-gauge needle (0.51 mm diameter, Fisher) was attached to the stereotaxic holder and zeroed on Bregma. To give the lens a snug fit and reduce brain motion artifacts,

Author Manuscript Author Manuscript Author Manuscript Author Manuscript

the needle was inserted slowly to a depth of 0.1 mm higher than the final depth of the GRIN lens. After this needle was removed from the brain, the GRIN lens was held with a bulldog serrafine clamp (Fine Science Tools, catalog no. 18050–28) with heat shrink on the tips (to improve grip and prevent damage) and zeroed at Bregma without touching the skull (to avoid debris covering the lens surface). The lens was then slowly inserted in the hole made by the needle and down to its final depth, then secured to the skull by applying Metabond (Parkell) or ultraviolet-curable glue (Loctite) around the lens. A titanium headplate was centered over the GRIN lens and fixed to the skull using Metabond. Afterwards, a 3D-printed plastic funnel was cemented onto the headplate, which allowed the securing of a light shield between the head and the objective using Velcro, to prevent collection of stray light. After completion of the GRIN lens surgery, the top of the GRIN lens was protected by a cut-off tip of an Eppendorf tube (Fisher) and secured using Kwik-Cast (WPI). The mice were allowed to recover from surgery for at least 2 weeks before any behavioral experiments.

Slice Electrophysiology—Ex vivo murine brain slices were prepared by deeply anesthetizing animals (6–8 weeks old) with isoflurane followed by rapid decapitation. Upon removal, brains were immediately immersed in ice-cold, carbogen-saturated (95% O2, 5% CO2) choline-based cutting solution consisting of (in mM): 92 choline chloride, 10 HEPES, 2.5 KCl, 1.25 NaH2PO4, 30 NaHCO3, 25 glucose, 10 MgSO4, 0.5 CaCl2, 2 thiourea, 5 sodium ascorbate, 3 sodium pyruvate, oxygenated with 95% O2/5% CO2, measured osmolarity 310 – 320 mOsm/L, pH= 7.4. Then, 275–300 mm-thick coronal sections containing the PBN complex were cut with a vibratome (Campden 7000smz-2) and incubated in oxygenated cutting solution at 34°C for 10 min. Next, slices were transferred to oxygenated aCSF (126 mM NaCl, 21.4 mM NaHCO3, 2.5 mM KCl, 1.2 mM NaH2PO4, 1.2 mM MgCl2, 2.4 mM CaCl2, 10 mM glucose) at 34°C for an additional 15 min. Slices were then kept at room temperature (20–24°C) for ^{3}45 min until use. A single slice was placed in the recording chamber where it was continuously superfused with oxygenated aCSF at a rate of 3–4 mL per min at room temperature. For Ca2+-free and Cd2+ recordings, slices were perfused with respective solutions for at least 10 min. Neurons were visualized with an upright microscope (Olympus) equipped with infrared-differential interference contrast and fluorescence optics.

Loose-seal, cell-attached recordings (seal resistance 20–50 MΩ) were made in voltage-clamp mode with the recording pipette filled with aCSF and holding current maintained at Vh = 0 mV. To photoactivate biPAC, a LED light source (470 nm) was used. The blue light was focused onto the back aperture of the microscope objective (40X) producing wide-field exposure around the recorded cell of 10–15 mW per mm2 as measured using an optical power peter (PM100D, Thorlabs). A programmable pulse stimulator, Master-8 (A.M.P.I.) and pClamp 10.2 software (Molecular Devices, Axon Instruments) controlled the photostimulation output.

Whole-cell patch clamp recordings in current clamp mode were used to record active membrane properties. Glutamatergic and GABAergic synaptic transmission was blocked using CNQX (10 μM) and D-APV (50 μM) or kynurenate (1 mM) and picrotoxin (100 μm) or bicuculline (10 μM) (“synaptic blockers”), respectively, in the bath solution to

Author Manuscript Author Manuscript Author Manuscript Author Manuscript

synaptically isolate patched PBN neurons. The recording pipette was filled with (in mM) 128 potassium gluconate, 10 KCl, 10 HEPES, 1 EGTA, 1 MgCl2, 0.3 CaCl2, 5 Na2-ATP, 0.3 NaGTP (pH 7.3). A series of depolarizing current steps (5 pA step; 0 to 60 pA, 4 s) was delivered from a holding potential of −70 mV. All recordings were made using a Multiclamp 700B amplifier and data were filtered at 2 kHz and digitized at 20 kHz. Recordings were analyzed offline using Clampfit 10

Freely moving feeding experiments with optogenetic stimulation—Mice were injected with biPAC bilaterally and a titanium headpost was cemented onto their skull. After 4 weeks of expression, mice were habituated to being connected to patch cords (bilateral, 400 μm core, 0.39 NA; Doric lenses) in their home cages (2 days; 1 – 2 hours per day). 24 hours before a test session, all food and bedding were removed from the cage and replaced with fresh bedding without food. During the test session, these mice were connected to patch cords in their home cage and provided with a single ~3 g standard chow pellet that was weighed beforehand. The pellet was then weighed every 30 minutes for 2 hours during which time the mice remained either unstimulated or received photostimulation either for 90 minutes following a 30-minute unstimulated period (100 ms pulse every 10 seconds; 1 mW 473 nm laser; LaserGlow) or during the first 30 minutes only (1 ms pulse every 10 seconds; 5 mW 473 nm laser; LaserGlow).

Head-fixed feeding experiments with optogenetic stimulation or tail shocks—We used a head-fixed behavioral paradigm[59,60] to achieve a higher temporal resolution assessment of the influence of photostimulation on feeding. Following freely moving photostimulation experiments, the same mice were habituated to head-fixation for 2 days. Mice were then maintained on a food restricted diet and trained to lick at a lick spout to receive Ensure. Following 2 days of habituation to the lick spout, mice were allowed to consume Ensure freely for 20 minutes. On test days with photostimulation, mice received 5 photostimulation trains (1 s on, 2 s off, 10 second duration, 1 mW, 465 nm LED; Plexon; two minute inter-train interval).

For experiments testing the effect of tail shock on feeding behavior, a separate cohort of mice were prepared with headpost implants only. Mice were chronically food restricted and trained to lick to receive Ensure as described above. On test days, mice received a 10 second duration tail shock train (6 Hz; 0.35 mA) that began 2 minutes after onset of free binging on Ensure. During initial experiments, we repeated this tail shock stimulus 5 times (2 minute intervals). In most experiments after the initial 5 mice, we only used a single tail shock train per trial and allowed several minutes breaks between trials to ensure the presence of multiple trials with stable licking before a tail shock (typically 2 – 3 trials per day). Locomotion was recorded using an IR sensor connected to an Arduino. The sensor detects crossings from a 3D-printed wheel that the mouse is running on as, in prior studies from our lab[59].

To test the role of cAMP signaling on the duration of tail shock-evoked suppression of feeding, we performed unilateral viral injections of a cre-dependent AAV-PDE4D3-Cat, a constitutively active phosphodiesterase that should selectively disrupt cAMP only[3]. We chose to use unilateral injections as we found that bilateral expression of PDE4D3-Cat in PBN neurons led to high mortality of the mice. Following five weeks of expression, mice

Author Manuscript Author Manuscript Author Manuscript Author Manuscript

were tested on the licking behavior as described above. We compared these animals to a set of control mice that expressed hM4Di-mCherry in PBN neurons but that were not injected with CNO. Post hoc histological analysis showed no obvious cell death resulting from expression of PDE4D3-Cat.

Real-time place aversion experiments—Mice were injected with biPAC virus (AAV1-hSYN-DIO-biPAC-WPRE) bilaterally targeting the PBN and optical fibers (200 μm core; 0.39 NA; R-FOC-L200C-39NA; RWD) were implanted bilaterally above the PBN. Following 4 weeks of expression, mice were fasted for 24 hours and tested in a re-feeding assay to confirm suppression of feeding upon biPAC stimulation (5 mW, 473 nm laser; 2 second ON; 8 second OFF). All seven mice showed complete suppression of feeding and were next tested for place aversion.

Mice were habituated for 2 days (one 20 minute session / day) in a rectangular arena (510 mm long, 270 mm wide, 300 mm tall) arena that was divided in the middle by a partial wall. An overhead camera (Microsoft USB webcam) and mouse tracking software (EthoVision; Version 14) were used to track animal movement and perform closed-loop photostimulation. On each of three testing days, mice were first recorded in the chamber for 10 minutes with no photostimulation. Afterwards, the left side of the arena was designated as the active side, in that photostimulation was triggered on all frames where the entirety of the mouse was on the left side (20 Hz, 2 mW; 473 nm LaserGlow laser). We quantified locomotion speed and time spent on each side of the arena over the course of these three days. We also used this arena and tracking software to determine locomotor effects of various photostimulation protocols.

Analysis of head-fixed licking behavior—For statistical analysis of the influence of manipulations (photostimulation or tail shock trains) on ongoing binge licking, we compared licking during the 1 minute (for photostimulation experiments) or 2 minutes (tail shock experiments) following the manipulation vs. the same window of time in unstimulated control sessions.

Characterization of PDE4D3-Cat expression—To quantify cell density in PDE4D3-Cat and control hemispheres, we took 3 consecutive 60 μm coronal brain slices centered on the PDE4D3 viral injection site. We segmented the regions of viral spread (red reporter expression) and trained a Cellpose[61] model to quantify DAPI nuclei within the segmented region. The same procedure was carried out for a region of equal shape and size applied to the non-injected hemisphere. The average per hemisphere for each group of 3 sections was then compared between PDE4D3 and control conditions.

Two-photon imaging via GRIN lenses—Two-photon imaging was performed using a resonant-scanning two-photon microscope (Neurolabware) at 15.5 frames s^{-1} and 796 × 512 pixels per frame as described previously[2,59]. Excitation was achieved using an InSight X3 laser (Spectra-Physics). Imaging was performed with a 10× 0.5 NA air objective (TL10X-2P; ThorLabs). Imaging fields of view were at a depth of 100–300 μm below the face of the GRIN lens and targeted the dorsal lateral subregion of lPBN (4 mice) or the external lateral subregion of lPBN (3 mice; ad libitum fed). We imaged using an excitation

Author Manuscript Author Manuscript Author Manuscript Author Manuscript

wavelength of 960 nm for all GCaMP or cADDis imaging, and 1100 nm for measuring mKate2 fluorescence as a proxy for biPAC protein expression. Laser power ranged between 40–60 mW at the front aperture of the objective (the power at the sample was substantially less because of partial transmission via the GRIN lens).

Two-photon imaging of acute brain slices.—For two-photon imaging of acute brain slices, slices were prepared as described above and transferred to a recording chamber perfused with ACSF (oxygenated with 95% O2 and 5% CO2; flow rate: 2–5 mL/min) at room temperature. All mice used for slice experiments were fed ad libitum. Imaging was performed with a 16× 0.8 NA water-immersion objective (Nikon). The excitation wavelength used was 920 nm. Field of view size was typically 900 × 600 μm^2. For optogenetic experiments involving biPAC, the PMT was powered off during the photostimulation (100 ms to 2 s; 470 nm LED; 1 mW/mm^2, Luxeon Star LEDs). LED photostimulation was driven by an Arduino-controlled driver (Luxeon Star LEDs).

For all pharmacological manipulations we collected pre- and post-drug responses to biPAC stimulation in the same cells. To block sodium channels, we applied tetrodotoxin (TTX, Sigma Aldrich, 2 μM in ACSF). To block PKA activity, we used a mixture of myristoylated protein kinase A inhibitor (PKI, 800 nM) and H89 (10 μM). To block hyperpolarization-activated cyclic nucleotide-gated channels, we used the selective blocker ZD7288 (50 μM, Tocris). To block excitatory transmission, we used CNQX (10 μM), and D-APV (20 μM). The cocktail condition included PKI (800 nM), H89 (10 μM), ZD7288 (50 μM), and the cyclic nucleotide gated channel blocker l-cis-diltiazem (LCD50 μM, Tocris). All drugs were applied for 10 minutes before starting a new biPAC stimulation trial.

Two-photon *in vitro* and *in vivo* image processing—Image registration for all two-photon calcium imaging of cell bodies was performed using Suite2p[62]. For extraction of signals from cell body regions of interest (ROIs) from volumetric brain slice imaging (15 depths spaced 10 μm apart), we used CellPose[61], which optimally identified ROIs of GCaMP- or cADDis-expressing cell bodies from the mean image of the movement-corrected field of view. Fluorescence time series were extracted by averaging each of the pixels within each binarized mask. We calculated neuropil activity as the median value of an annulus surrounding each ROI (inner radius: 15 pixels; outer radius: 50 pixels; 0.85 pixels/μm, pixels belonging to any other ROI were excluded from these annulus masks).

Two-photon data analysis—This time course of neuropil activity was subtracted from the activity time course of the associated ROI to create a fluorescence time course, F(t), where t is the time of each imaging frame. The change in fluorescence was calculated by subtracting a running estimate of baseline fluorescence ($F_0(t)$) from F(t), then dividing by $F_0(t)$: $dF/F(t) = (F(t) - F_0(t))/F_0(t)$, where $F_0(t)$ is the average fluorescence in a 30 second window prior to biPAC stimulation, or in a 5-minute window prior to drug application.

Significantly responding neurons (in the case of both cADDis and GCaMP) were defined as neurons whose post-stimulation fluorescence, averaged across the first 30 seconds after the blue light pulse, exceeded baseline fluorescence in the 30 seconds prior to stimulation by 1 standard deviation and 5% dF/F. Of note, cADDis is a downwards sensor (i.e., it signals

Author Manuscript Author Manuscript Author Manuscript Author Manuscript

through fluorescence decreases), so we have flipped all cADDis traces and signals to be positive for ease of visualization throughout the paper.

To calculate the duration of GCaMP responses to biPAC stimulation or Forskolin application, we calculated the amount of time that each neuron's GCaMP fluorescence exceeded a pre-determined threshold (exceeding the fluorescence level during the 30 second baseline period by at least 1 standard deviation and 5% dF/F) until the first time it returned below this threshold for at least 20 consecutive seconds.

To quantify the rate of clearance of cAMP in each neuron, we used the following formula:

$$N(t) = N_0 e^{-t/\tau}$$

We chose N_0 as 80% of peak actual cADDis fluorescence, and fit for the decay time constant, τ, using all time points with associated fluorescence values spanning 20–80% of peak fluorescence.

Statistics—No statistical methods were used to pre-determine sample sizes, but our sample sizes were chosen to reliably measure experimental parameters while remaining in compliance with ethical guidelines for minimizing animal use, and were similar to those reported in previous publications. Experiments were conducted by an investigator with knowledge of the animal genotype and treatment. All the virus expression, optic fiber implants and GRIN lens placements were verified by post hoc histology or were verified during the experiment (slice imaging). All data presented as bar and line graphs indicate mean ± s.e.m., with individual data points also plotted. Parametric statistical tests were used in most cases. In some, linear mixed effect models were used (see below). Statistical analyses were performed in Matlab (Mathworks) or GraphPad Prism (version 10). Significance levels are indicated as follows unless otherwise specified: *p< 0.05; **p< 0.01; ***p< 0.001.

Mixed-effects models—Linear mixed effects models (LMEMs) were computed in Matlab. LMEMs were used to account for the hierarchical dependencies in the data (neurons -> slices -> mice), particularly when a large sample of neurons was being compared across conditions. Specifically, we accounted for correlations between measurements that were sampled from the same slice by including fixed effect terms for slice ID and for mouse ID. Fixed effect coefficient and p values are reported in the main text and figures.

Supplementary Material

Refer to Web version on PubMed Central for supplementary material.

Acknowledgements

We thank B. Lowell, M. Krashes, S. Liu, S. Zhang, R. Essner, K. Ruda and the Andermann and Lutas labs for useful feedback. We also thank S. Zhang for technical assistance with biPAC stimulation experiments. Authors were supported by NIH F32 DK112589, a Davis Family Foundation award, a BNORC pilot grant (P30DK046200), and ZIA DK075169 (A.L.); a Harvard Mind Brain and Behavior postdoctoral fellowship (J.S.A), NIH R01 DK109930, DP1 AT010971, R01 MH12343, a McKnight Scholar Award, and grants from the Boston Nutrition and Obesity

Author Manuscript Author Manuscript Author Manuscript Author Manuscript

Research Center (P30 DK046200), The Pew Innovation Fund, and the Klarman Family Foundation (M.L.A.); and the Boston Children's Hospital Viral Core for virus packaging (NIH P30 EY012196).

References

1. Tewson P, Martinka S, Shaner N, Berlot C, Quinn AM, and Hughes T. (2018). Assay for Detecting Gαi-Mediated Decreases in cAMP in Living Cells. SLAS Discov 23, 898–906. [PubMed: 29991302]
2. Lutas A, Fernando K, Zhang SX, Sambangi A, and Andermann ML (2022). History-dependent dopamine release increases cAMP levels in most basal amygdala glutamatergic neurons to control learning. Cell Rep. 38, 110297.
3. Zhang SX, Lutas A, Yang S, Diaz A, Fluhr H, Nagel G, Gao S, and Andermann ML (2021). Hypothalamic dopamine neurons motivate mating through persistent cAMP signalling. Nature 597, 245– 249. [PubMed: 34433964]
4. Ma L, Day-Cooney J, Benavides OJ, Muniak MA, Qin M, Ding JB, Mao T, and Zhong H. (2022). Locomotion activates PKA through dopamine and adenosine in striatal neurons. Nature 611, 762–768. [PubMed: 36352228]
5. Lee SJ, Lodder B, Chen Y, Patriarchi T, Tian L, and Sabatini BL (2021). Cell-type-specific asynchronous modulation of PKA by dopamine in learning. Nature 590, 451–456. [PubMed: 33361810]
6. Yagishita S, Hayashi-Takagi A, Ellis-Davies GCR, Urakubo H, Ishii S, and Kasai H. (2014). A critical time window for dopamine actions on the structural plasticity of dendritic spines. Science 345, 1616–1620. [PubMed: 25258080]
7. Thornquist SC, Pitsch MJ, Auth CS, and Crickmore MA (2021). Biochemical evidence accumulates across neurons to drive a network-level eruption. Mol. Cell 81, 675–690.e8.
8. Karthik S, Huang D, Delgado Y, Laing JJ, Peltekian L, Iverson GN, Grady F, Miller RL, McCann CM, Fritzsch B, et al. (2022). Molecular ontology of the parabrachial nucleus. J. Comp. Neurol. 530, 1658–1699. [PubMed: 35134251]
9. Pauli JL, Chen JY, Basiri ML, Park S, Carter ME, Sanz E, McKnight GS, Stuber GD, and Palmiter RD (2022). Molecular and anatomical characterization of parabrachial neurons and their axonal projections. Elife 11. 10.7554/eLife.81868.
10. Nardone S., De Luca R., Zito A., Klymko N., Nicoloutsopoulos D., Amsalem O., Brannigan C., Resch JM., Jacobs CL., Pant D., et al. . (2023). A spatially-resolved transcriptional atlas of the murine dorsal pons at single-cell resolution. bioRxiv, 2023.09.18.558047. 10.1101/2023.09.18.558047.
11. Carter ME, Soden ME, Zweifel LS, and Palmiter RD (2013). Genetic identification of a neural circuit that suppresses appetite. Nature 503, 111–114. [PubMed: 24121436]
12. Sun L, Liu R, Guo F, Wen M-Q, Ma X-L, Li K-Y, Sun H, Xu C-L, Li Y-Y, Wu M-Y, et al. (2020). Parabrachial nucleus circuit governs neuropathic pain-like behavior. Nat. Commun. 11, 5974. [PubMed: 33239627]
13. Xie Z, Zhang X, Zhao M, Huo L, Huang M, Li D, Zhang S, Cheng X, Gu H, Zhang C, et al. (2022). The gut-to-brain axis for toxin-induced defensive responses. Cell 185, 4298–4316.e21.
14. Chen JY, Campos CA, Jarvie BC, and Palmiter RD (2018). Parabrachial CGRP Neurons Establish and Sustain Aversive Taste Memories. Neuron 100, 891–899.e5.
15. Campos CA, Bowen AJ, Roman CW, and Palmiter RD (2018). Encoding of danger by parabrachial CGRP neurons. Nature 555, 617–622. [PubMed: 29562230]
16. Barik A, Thompson JH, Seltzer M, Ghitani N, and Chesler AT (2018). A Brainstem-Spinal Circuit Controlling Nocifensive Behavior. Neuron 100, 1491–1503.e3.
17. Alhadeff AL, Su Z, Hernandez E, Klima ML, Phillips SZ, Holland RA, Guo C, Hantman AW, De Jonghe BC, and Betley JN (2018). A Neural Circuit for the Suppression of Pain by a Competing Need State. Cell 173, 140–152.e15.
18. Chiang MC, Nguyen EK, Canto-Bustos M, Papale AE, Oswald A-MM, and Ross SE (2020). Divergent Neural Pathways Emanating from the Lateral Parabrachial Nucleus Mediate Distinct Components of the Pain Response. Neuron 106, 927–939.e5.

Author Manuscript Author Manuscript Author Manuscript Author Manuscript

19. Raver C, Uddin O, Ji Y, Li Y, Cramer N, Jenne C, Morales M, Masri R, and Keller A. (2020). An Amygdalo-Parabrachial Pathway Regulates Pain Perception and Chronic Pain. J. Neurosci. 40, 3424– 3442. [PubMed: 32217613]
20. Bowen AJ, Chen JY, Huang YW, Baertsch NA, Park S, and Palmiter RD (2020). Dissociable control of unconditioned responses and associative fear learning by parabrachial CGRP neurons. Elife 9. 10.7554/eLife.59799.
21. Condon LF., Yu Y., Park S., Cao F., Pauli JL., Nelson TS., and Palmiter RD. (2023). Parabrachial Calca neurons drive nociplasticity. bioRxiv, 2023.10.26.564223. 10.1101/2023.10.26.564223.
22. Yang B, Sanches-Padilla J, Kondapalli J, Morison SL, Delpire E, Awatramani R, and Surmeier DJ (2021). Locus coeruleus anchors a trisynaptic circuit controlling fear-induced suppression of feeding. Neuron 109, 823–838.e6.
23. Nagashima T, Tohyama S, Mikami K, Nagase M, Morishima M, Kasai A, Hashimoto H, and Watabe AM (2022). Parabrachial-to-parasubthalamic nucleus pathway mediates fear-induced suppression of feeding in male mice. Nat. Commun. 13, 7913. [PubMed: 36585411]
24. Phua SC, Tan YL, Kok AMY, Senol E, Chiam CJH, Lee C-Y, Peng Y, Lim ATJ, Mohammad H, Lim J-X, et al. (2021). A distinct parabrachial-to-lateral hypothalamus circuit for motivational suppression of feeding by nociception. Sci Adv 7. 10.1126/sciadv.abe4323.
25. Roman CW, Derkach VA, and Palmiter RD (2016). Genetically and functionally defined NTS to PBN brain circuits mediating anorexia. Nat. Commun. 7, 11905.
26. Wu Q, Clark MS, and Palmiter RD (2012). Deciphering a neuronal circuit that mediates appetite. Nature 483, 594–597. [PubMed: 22419158]
27. Han Y, Xia G, He Y, He Y, Farias M, Xu Y, and Wu Q. (2021). A hindbrain dopaminergic neural circuit prevents weight gain by reinforcing food satiation. Sci Adv 7. 10.1126/sciadv.abf8719.
28. Zhang J-F, Liu B, Hong I, Mo A, Roth RH, Tenner B, Lin W, Zhang JZ, Molina RS, Drobizhev M, et al. (2021). An ultrasensitive biosensor for high-resolution kinase activity imaging in awake mice. Nat. Chem. Biol. 17, 39–46. [PubMed: 32989297]
29. Zhang SX, Kim A, Madara JC, Zhu PK, Christenson LF, Lutas A, Kalugin PN, Jin Y, Pal A, Tian L, et al. (2023). Competition between stochastic neuropeptide signals calibrates the rate of satiation. bioRxiv, 2023.07.11.548551. 10.1101/2023.07.11.548551.
30. Porro A, Saponaro A, Gasparri F, Bauer D, Gross C, Pisoni M, Abbandonato G, Hamacher K, Santoro B, Thiel G, et al. (2019). The HCN domain couples voltage gating and cAMP response in hyperpolarization-activated cyclic nucleotide-gated channels. Elife 8. 10.7554/eLife.49672.
31. Wainger BJ., DeGennaro M., Santoro B., Siegelbaum SA., and Tibbs GR. (2001). Molecular mechanism of cAMP modulation of HCN pacemaker channels. Nature 411, 805–810. [PubMed: 11459060]
32. Podda MV, D'Ascenzo M, Leone L, Piacentini R, Azzena GB, and Grassi C. (2008). Functional role of cyclic nucleotide-gated channels in rat medial vestibular nucleus neurons. J. Physiol. 586, 803–815. [PubMed: 18048449]
33. Yovell Y, and Abrams TW (1992). Temporal asymmetry in activation of Aplysia adenylyl cyclase by calcium and transmitter may explain temporal requirements of conditioning. Proc. Natl. Acad. Sci. U. S. A. 89, 6526–6530. [PubMed: 1631153]
34. Ji Y, Onwukwe C, Smith J, Laub H, Posa L, Keller A, Masri R, and Cramer N. (2023). Noradrenergic Input from Nucleus of the Solitary Tract Regulates Parabrachial Activity in Mice. eNeuro 10. 10.1523/ENEURO.0412-22.2023.
35. Li H, and Li YQ (2000). Collateral projection of substance P receptor expressing neurons in the medullary dorsal horn to bilateral parabrachial nuclei of the rat. Brain Res. Bull. 53, 163–169. [PubMed: 11044592]
36. Blomqvist A, and Mackerlova L. (1995). Spinal projections to the parabrachial nucleus are substance P-immunoreactive. Neuroreport 6, 605–608. [PubMed: 7541653]
37. Deng J, Zhou H, Lin J-K, Shen Z-X, Chen W-Z, Wang L-H, Li Q, Mu D, Wei Y-C, Xu X-H, et al. (2020). The Parabrachial Nucleus Directly Channels Spinal Nociceptive Signals to the Intralaminar Thalamic Nuclei, but Not the Amygdala. Neuron 107, 909–923.e6.

Author Manuscript Author Manuscript Author Manuscript Author Manuscript

38. Liu S, Kim D-I, Oh TG, Pao GM, Kim J-H, Palmiter RD, Banghart MR, Lee K-F, Evans RM, and Han S. (2021). Neural basis of opioid-induced respiratory depression and its rescue. Proc. Natl. Acad. Sci. U. S. A. 118. 10.1073/pnas.2022134118.
39. Han S, Soleiman MT, Soden ME, Zweifel LS, and Palmiter RD (2015). Elucidating an Affective Pain Circuit that Creates a Threat Memory. Cell 162, 363–374. [PubMed: 26186190]
40. Kakkar R, Raju RV, and Sharma RK (1999). Calmodulin-dependent cyclic nucleotide phosphodiesterase (PDE1). Cell. Mol. Life Sci. 55, 1164–1186. [PubMed: 10442095]
41. Ster J, De Bock F, Guérineau NC, Janossy A, Barrère-Lemaire S, Bos JL, Bockaert J, and Fagni L. (2007). Exchange protein activated by cAMP (Epac) mediates cAMP activation of p38 MAPK and modulation of Ca2+-dependent K+ channels in cerebellar neurons. Proc. Natl. Acad. Sci. U. S. A. 104, 2519–2524. [PubMed: 17284589]
42. Shariati B, Thompson EL, Nicol GD, and Vasko MR (2016). Epac activation sensitizes rat sensory neurons through activation of Ras. Mol. Cell. Neurosci. 70, 54–67. [PubMed: 26596174]
43. Liu S, Ye M, Pao GM, Song SM, Jhang J, Jiang H, Kim J-H, Kang SJ, Kim D-I, and Han S. (2022). Divergent brainstem opioidergic pathways that coordinate breathing with pain and emotions. Neuron 110, 857–873.e9.
44. Kaur S, Wang JL, Ferrari L, Thankachan S, Kroeger D, Venner A, Lazarus M, Wellman A, Arrigoni E, Fuller PM, et al. (2017). A Genetically Defined Circuit for Arousal from Sleep during Hypercapnia. Neuron 96, 1153–1167.e5.
45. Alhadeff AL, Holland RA, Nelson A, Grill HJ, and De Jonghe BC (2015). Glutamate Receptors in the Central Nucleus of the Amygdala Mediate Cisplatin-Induced Malaise and Energy Balance Dysregulation through Direct Hindbrain Projections. J. Neurosci. 35, 11094–11104.
46. Campos CA, Bowen AJ, Han S, Wisse BE, Palmiter RD, and Schwartz MW (2017). Cancer-induced anorexia and malaise are mediated by CGRP neurons in the parabrachial nucleus. Nat. Neurosci. 20, 934–942. [PubMed: 28581479]
47. Yang WZ, Du X, Zhang W, Gao C, Xie H, Xiao Y, Jia X, Liu J, Xu J, Fu X, et al. (2020). Parabrachial neuron types categorically encode thermoregulation variables during heat defense. Sci Adv 6. 10.1126/sciadv.abb9414.
48. Jung S, Lee M, Kim D-Y, Son C, Ahn BH, Heo G, Park J, Kim M, Park H-E, Koo D-J, et al. (2022). A forebrain neural substrate for behavioral thermoregulation. Neuron 110, 266–279.e9.
49. Myers MG Jr, Affinati AH, Richardson N, and Schwartz MW. (2021). Central nervous system regulation of organismal energy and glucose homeostasis. Nat Metab 3, 737–750. [PubMed: 34158655]
50. Rodriguez E, Ryu D, Zhao S, Han B-X, and Wang F. (2019). Identifying Parabrachial Neurons Selectively Regulating Satiety for Highly Palatable Food in Mice. eNeuro 6. 10.1523/ENEURO.0252-19.2019.
51. Campos CA., Bowen AJ., Schwartz MW., and Palmiter RD. (2016). Parabrachial CGRP Neurons Control Meal Termination. Cell Metab. 23, 811–820. [PubMed: 27166945]
52. Alhadeff AL, Baird J-P, Swick JC, Hayes MR, and Grill HJ (2014). Glucagon-like Peptide-1 receptor signaling in the lateral parabrachial nucleus contributes to the control of food intake and motivation to feed. Neuropsychopharmacology 39, 2233–2243. [PubMed: 24681814]
53. Alhadeff AL, Hayes MR, and Grill HJ (2014). Leptin receptor signaling in the lateral parabrachial nucleus contributes to the control of food intake. Am. J. Physiol. Regul. Integr. Comp. Physiol. 307, R1338–44. [PubMed: 25298514]
54. Barik A, Sathyamurthy A, Thompson J, Seltzer M, Levine A, and Chesler A. (2021). A spinoparabrachial circuit defined by Tacr1 expression drives pain. Elife 10. 10.7554/eLife.61135.
55. Uddin O, Studlack P, Akintola T, Raver C, Castro A, Masri R, and Keller A. (2018). Amplified parabrachial nucleus activity in a rat model of trigeminal neuropathic pain. Neurobiol Pain 3, 22–30. [PubMed: 29862375]
56. Cramer N, Silva-Cardoso G, Masri R, and Keller A. (2021). Control of synaptic transmission and neuronal excitability in the parabrachial nucleus. Neurobiol Pain 9, 100057.
57. Lodder B, Lee SJ, and Sabatini BL (2021). Real-Time, In Vivo Measurement of Protein Kinase A Activity in Deep Brain Structures Using Fluorescence Lifetime Photometry (FLiP). Curr Protoc 1, e265. [PubMed: 34661994]

Author Manuscript Author Manuscript Author Manuscript Author Manuscript

58. Massengill CI, Bayless-Edwards L, Ceballos CC, Cebul ER, Cahill J, Bharadwaj A, Wilson E, Qin M, Whorton MR, Baconguis I, et al. (2022). Sensitive genetically encoded sensors for population and subcellular imaging of cAMP in vivo. Nat. Methods 19, 1461–1471. [PubMed: 36303019]

59. Lutas A, Kucukdereli H, Alturkistani O, Carty C, Sugden AU, Fernando K, Diaz V, Flores-Maldonado V, and Andermann ML (2019). State-specific gating of salient cues by midbrain dopaminergic input to basal amygdala. Nat. Neurosci. 22, 1820–1833. [PubMed: 31611706]

60. Burgess CR, Ramesh RN, Sugden AU, Levandowski KM, Minnig MA, Fenselau H, Lowell BB, and Andermann ML (2016). Hunger-Dependent Enhancement of Food Cue Responses in Mouse Postrhinal Cortex and Lateral Amygdala. Neuron 91, 1154–1169. [PubMed: 27523426]

61. Stringer C, Wang T, Michaelos M, and Pachitariu M. (2021). Cellpose: a generalist algorithm for cellular segmentation. Nat. Methods 18, 100–106. [PubMed: 33318659]

62. Pachitariu M., Stringer C., Schröder S., Dipoppa M., Federico Rossi L., Carandini M., and Harris KD. (2016). Suite2p: beyond 10,000 neurons with standard two-photon microscopy. BioRxiv, 061507.

Author Manuscript Author Manuscript Author Manuscript Author Manuscript

Highlights

- Transient cAMP production drives minutes-long spiking in parabrachial nucleus neurons
- Translation of cAMP to spiking relies on PKA-dependent and independent mechanisms
- Shock-evoked cAMP is necessary for prolonged pain-induced suppression of feeding
- cAMP signaling extends behavioral responses to threat stimuli from seconds to minutes

Author Manuscript
Author Manuscript
Author Manuscript
Author Manuscript

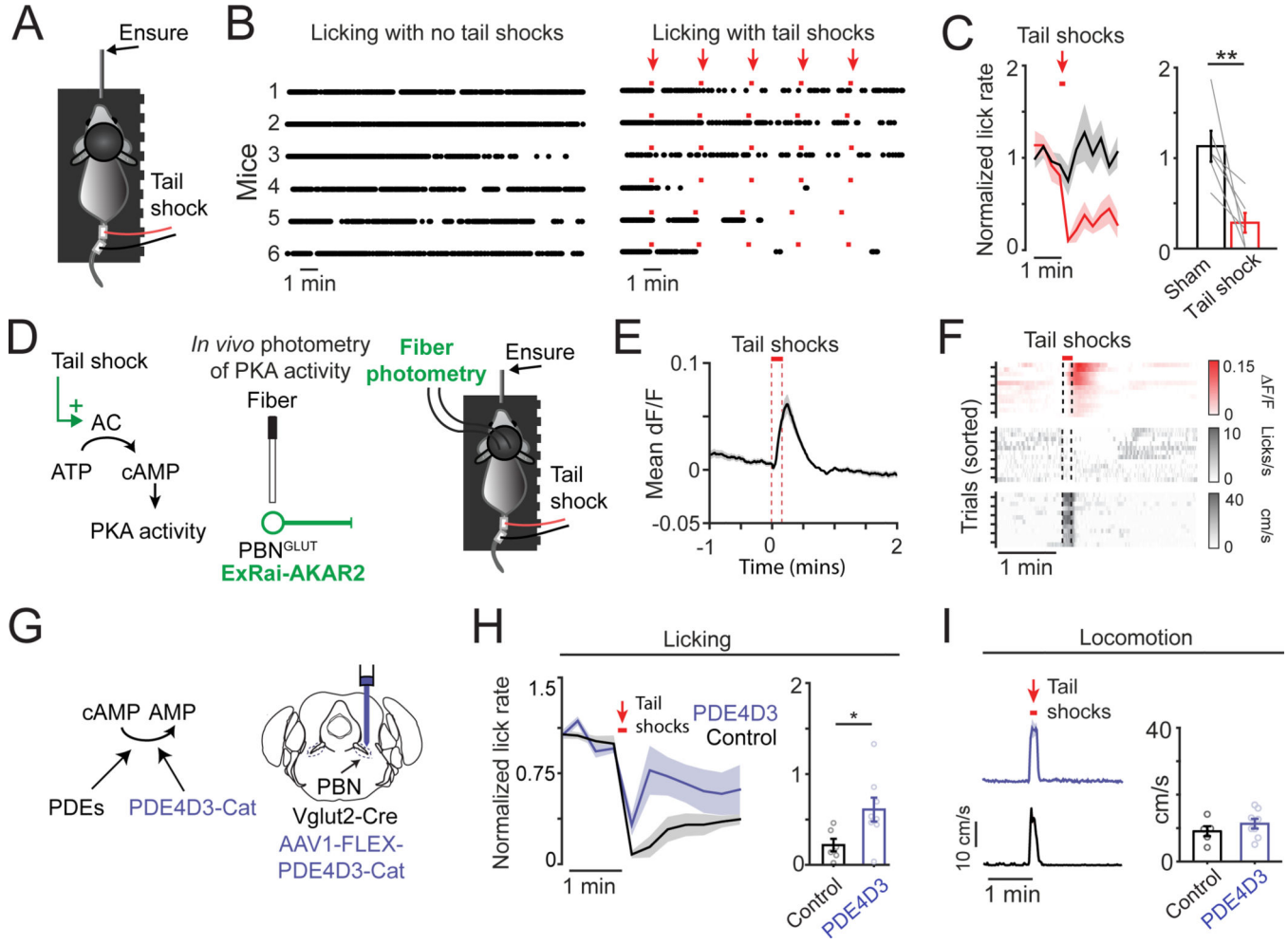

Figure 1: Brief, salient events halt feeding for extended periods via cAMP-dependent signaling in PBN^{Glut} neurons.

A) Schematic depicting head fixation on a treadmill during consumption of liquid food (Ensure) and tail shock delivery.

B) Left: licking during lick-triggered Ensure delivery on the control session (no tail shocks). Right: licking during test day with intermittent delivery of tail shocks (10 s; 6 Hz; 0.35 mA).

C) Left: time course of mean peak-normalized licking across mice (n = 6) in tail shock sessions (red) vs. sham controls (black). Right: mean normalized licking in the two-minute period following tail shock or sham. Two-tailed paired *t*-test, p = 0.007.

D) Left: schematic depicting predicted influence of tail shocks on adenylyl cyclase and PKA activity in PBN neurons. Middle and right: fiber photometry recording of ExRai-AKAR2 during Ensure consumption and tail shock.

E) Time course of mean peak-normalized PKA activity aligned to tail shock delivery (n = 4 mice).

F) Top: heatmap of normalized PKA activity (n = 12 trials from 4 mice) sorted by peak magnitude following tail shock. Lick rasters (middle) and locomotion (bottom), plotted with same sorting as top panel.

Author Manuscript Author Manuscript Author Manuscript Author Manuscript

G) Left: Schematic depicting PDE4D3-Cat effect on cAMP. Right: expression of PDE4D3-Cat unilaterally in PBN^{Glut} neurons.

H) Left: time course of mean normalized licking of Ensure and interruption by tail shocks in mice expressing PDE4D3-Cat (blue; n = 8 mice) or controls (black; n = 6 mice). Right: mean normalized licking in the two-minute period following tail shock or sham. Two-tailed unpaired *t*-test, p = 0.03.

I) Left: time course of mean locomotion (cm/s) for PDE4D3-Cat (blue) or control mice (black). Right: mean locomotion during tail shock. Two-tailed unpaired *t*-test, p = 0.42.

All data: mean ± s.e.m.

See also Supplemental Figures 1 and 2.

Author Manuscript
Author Manuscript
Author Manuscript
Author Manuscript

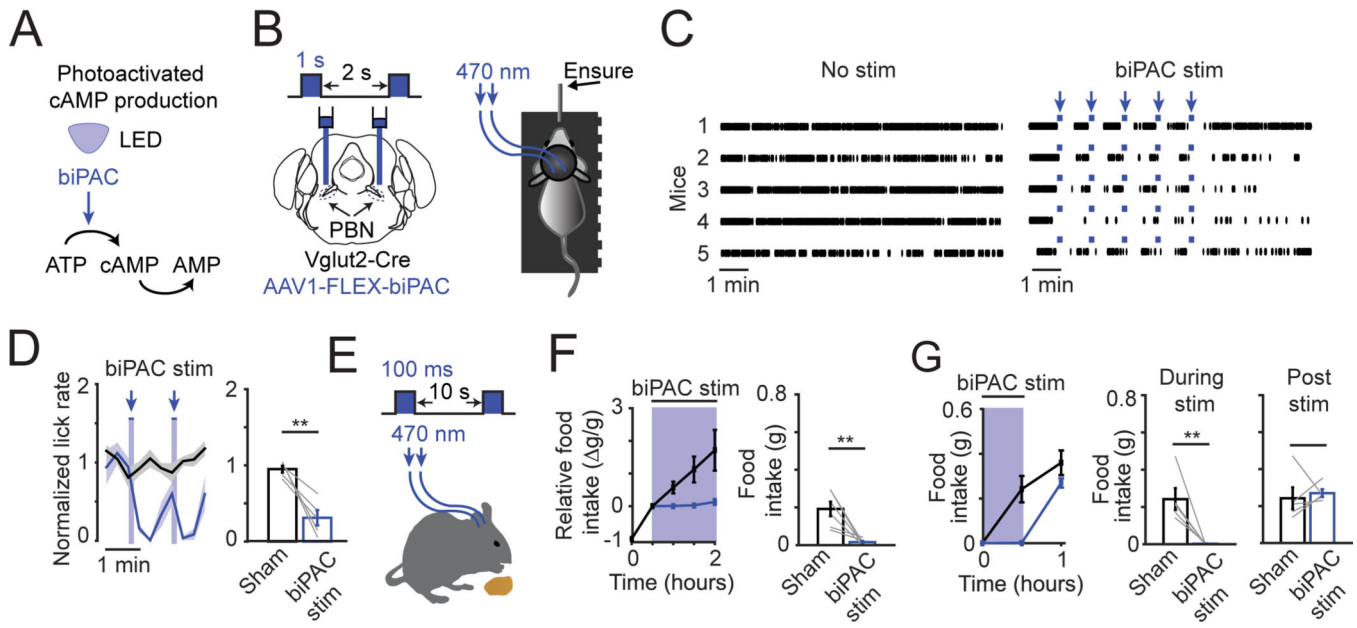

Figure 2: Transient photostimulated production of cAMP in PBN^{Glut} neurons suppresses food seeking for tens of seconds.

A) Schematic depicting photostimulation of cAMP production using biPAC, and subsequent degradation of cAMP to AMP.

B) Bilateral biPAC expression in PBN^{Glut} neurons and photostimulation paradigm (1 s LED on, 2 s LED off; 10 s duration) during Ensure consumption.

C) Licking during lick-triggered Ensure delivery on the control session (left; no photostimulation of biPAC) and on the test session (right; intermittent photostimulation).

D) Left: time course of mean normalized licking of mice (n = 5) on control (black; sham) or test sessions (blue; photostimulation). Right: mean normalized licking in the one-minute period following photostimulation or sham. Two-tailed paired *t*-test, p = 0.006.

E) Schematic depicting photostimulation of biPAC (100 ms LED on, 10 s LED off; 1 mW) during chow consumption in freely moving mice.

F) Left: food intake measurements over a two-hour session of refeeding in fasted mice without photostimulation (black; n = 6 mice) or with photostimulation (blue). Photostimulation started after the first 30 minutes. Right: mean food consumption during the last 90 minutes on control vs. test days. Two-tailed paired *t*-test, p = 0.009.

G) Left: food intake during the first hour of refeeding in fasted mice without photostimulation (black; n = 5 mice) or with photostimulation during the first 30 minutes of the hour (blue; 1-s LED on, 10-s off; 5 mW). Middle and right: mean food consumption during the 30 minutes of stimulation (middle; two-tailed paired *t*-test, p = 0.004) or 30 minutes after stimulation offset (right; p = 0.67) on control vs. on test days.

All data: mean ± s.e.m.

See also Supplemental Figures 1 and 2.

Author Manuscript Author Manuscript Author Manuscript Author Manuscript

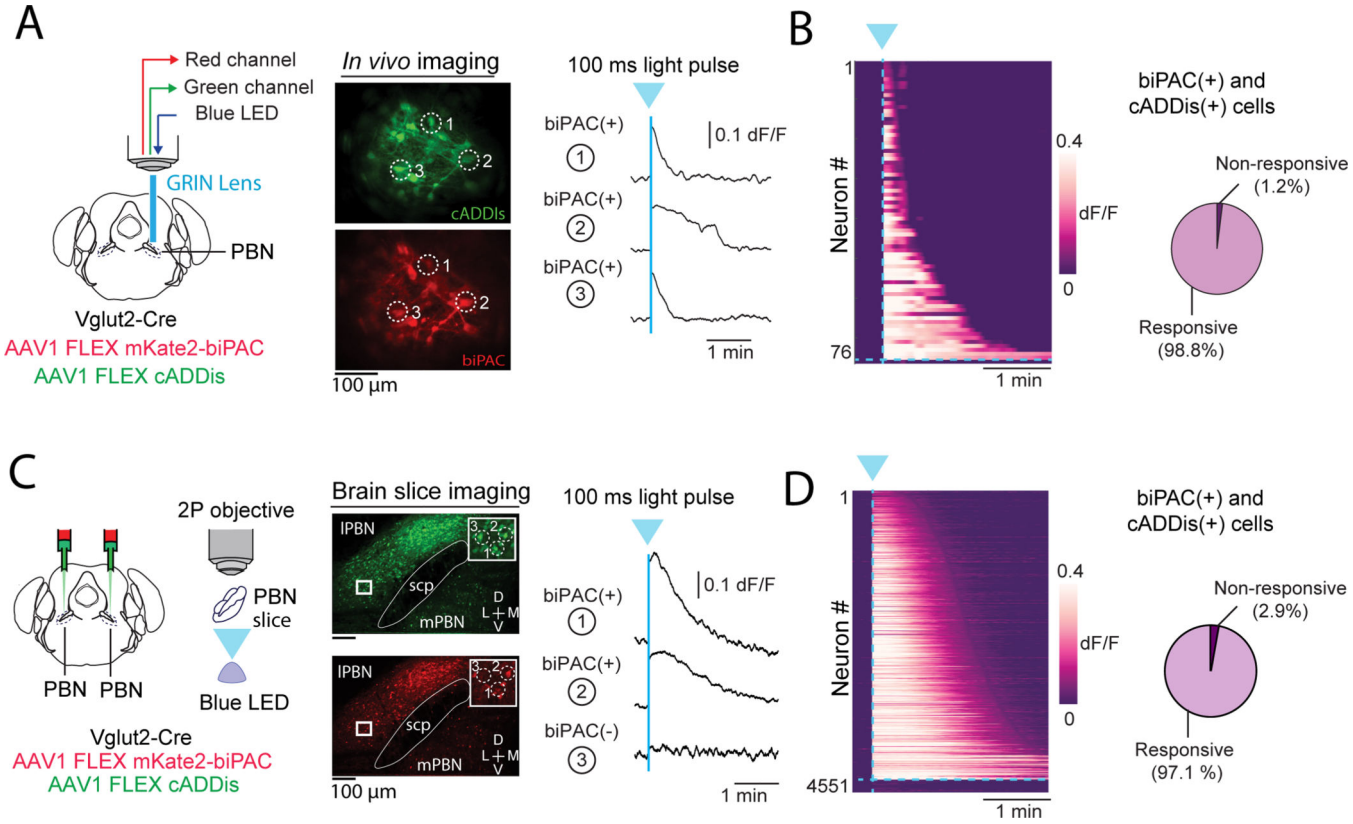

Figure 3: Photostimulated production of cAMP in PBN^{Glut} neurons persists for tens of seconds.

A) Left: *in vivo* two-photon imaging of cAMP using cADDis during brief photostimulaton of cAMP using biPAC (100 ms blue light pulse). Right: representative traces of cADDis fluorescence from 3 neurons.

B) Heatmap showing effect of biPAC stimulation on all imaged neurons (76 neurons, 4 mice). Right: fraction of neurons with responses to stimulation.

C) Left: similar to (A), but imaging in brain slices. Right: cADDis fluorescence traces from 2 example neurons expressing mKate2-biPAC (biPAC(+)) and one lacking mKate2-biPAC expression (biPAC(−)).

D) Heatmap showing effect of biPAC stimulation on all neurons (4551 neurons, 15 slices from 5 mice). Right: fraction of neurons with responses to stimulation.

See also Supplemental Figures 2 and 3.

Author Manuscript
Author Manuscript
Author Manuscript
Author Manuscript

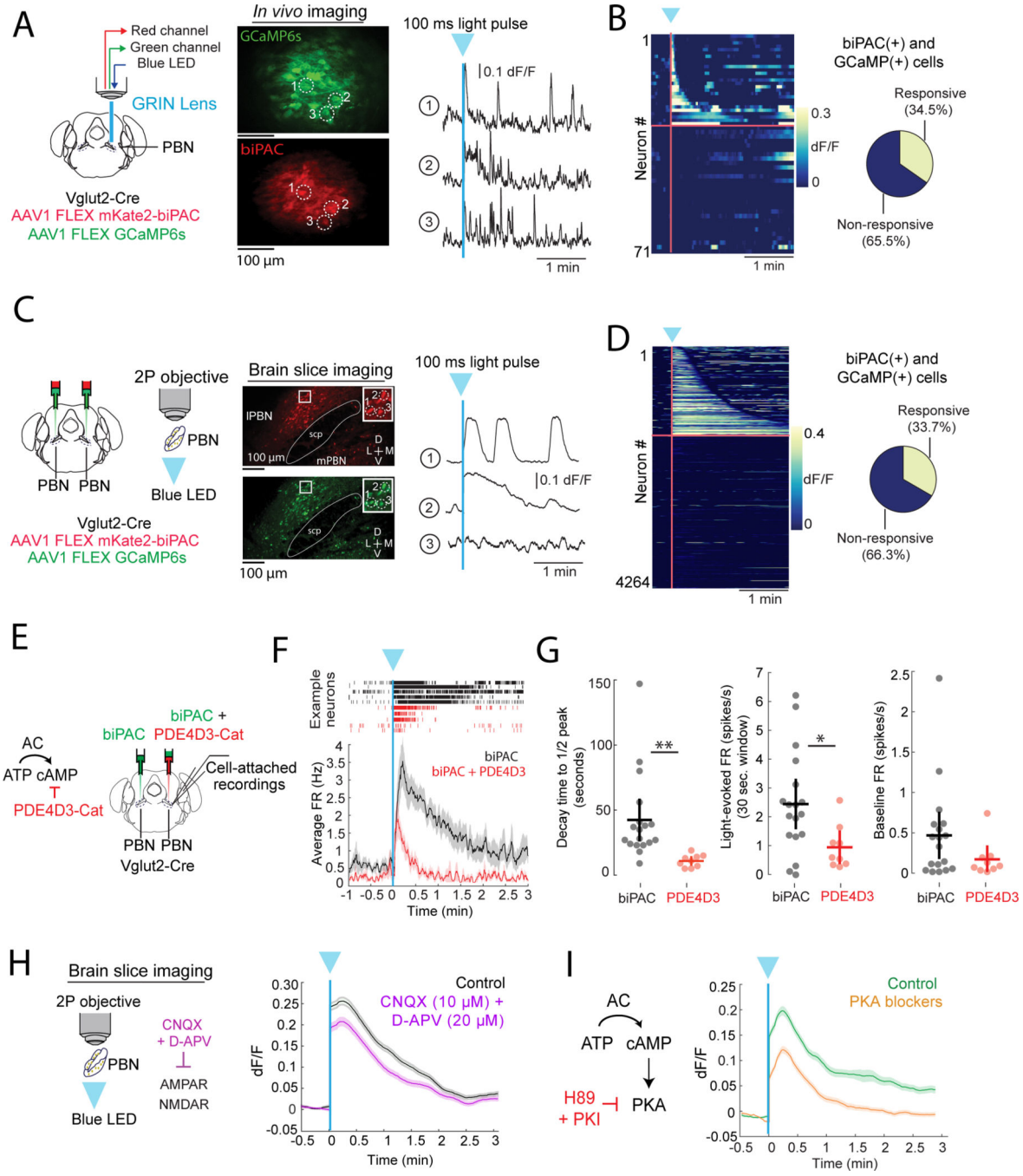

Figure 4: Photostimulation of cAMP drives persistent increases in spiking in some PBN^{Glut} neurons

A) Left: schematic depicting *in vivo* calcium imaging. Right: traces of GCaMP6s fluorescence from 3 neurons stimulated with blue light (100 ms pulse).

B) Heatmap of responses to biPAC stimulation across neurons (71 neurons, 4 mice). Right: fraction of neurons with responses to stimulation.

C) Left: similar to (A), but imaging in brain slices. Right: traces of GCaMP6s fluorescence from 3 neurons.

Author Manuscript Author Manuscript Author Manuscript Author Manuscript

D) Heatmap of responses to biPAC stimulation across neurons (4264 neurons, 17 slices, 5 mice). Right: fraction of neurons with responses to stimulation.
E) Viral infection strategy for cell-attached recordings in PBN.
F) Top: example neurons (5/condition) showing single-trial firing rate responses to blue light in the presence (red) or absence (black) of PDE4D3-Cat. Bottom: average firing rates across all recorded neurons.
G) Group data showing time to half peak (left; $^{**}p < 0.01$, two-tailed unpaired *t*-test), mean firing rate response (middle; $^{*}p < 0.05$), and mean baseline firing rate for control vs. PDE4D3-Cat conditions (right; $p = 0.16$).
H) Left: imaging during delivery of CNQX (10 μM) and D-APV (20 μM). Right: average GCaMP6s responses to biPAC stimulation in the absence or presence of CNQX and D-APV (954 responsive neurons, 3 slices from 3 mice).
I) Left: Illustration of effects of PKA inhibitors. Right: GCaMP6s responses to biPAC stimulation before and after PKA inhibitors (411 responsive neurons, 4 slices from 3 mice). Average baseline and biPAC-evoked dF/F are calculated in the 30 second window before and after stimulation respectively. All data: mean ± s.e.m.
See also Supplemental Figures 3 and 4.

Author Manuscript Author Manuscript Author Manuscript Author Manuscript

Key resources table

REAGENT or RESOURCE	SOURCE	IDENTIFIER
Bacterial and virus strains		
AAV2/1.hSyn.DIO.GreenDownwardcADDis.WPRE	Boston Children's Hospital Viral Core	Zhang et al., 2021
AAV2/1.EF1a.DIO.mKate2-biPAC.WPRE	Boston Children's Hospital Viral Core	Zhang et al., 2021
AAV2/1.EF1a.DIO.mKate2-PDE4D3-cat.WPRE	Boston Children's Hospital Viral Core	Zhang et al., 2021
AAV2/1.hSyn.FLEX.GCaMP6s.WPRE	Chen et al., 2013	Addgene Cat# 100845
AAV2/9.hSyn.FLEX.ExRai-AKAR2-CW3SL	Richard Huganir	Zhang et al., 2021
Chemicals, peptides, and recombinant proteins		
Forskolin	Tocris	Cat# 1099
CNQX disodium salt	Tocris	Cat# 1045
D-AP5	Tocris	Cat# 0106
Tetrodotoxin	Tocris	Cat# 1078
ZD7288	Tocris	Cat# 1000
Myristoylated PKI	Tocris	Cat# 2546
H-89 dihydrochloride	Tocris	Cat# 2910
L-cis-Diltiazem hydrochloride	Tocris	Cat# 0685
Experimental models: Organisms/strains		
Mouse: Vglut2-ires-cre; C57BL/6J	The Jackson Laboratory	RRID:IMSR_JAX:0 16963
Software and algorithms		
MATLAB R2022	Mathworks	https://www.mathworks.com/products/matlab.html; RRID:SCR_001622
Scanbox	Neurolabware	https://scanbox.org
Fiji	NIH	Schindelin et al., 2012
Other		
Two-photon microscope	Neurolabware	CAT# TL10X-2P
InSight X3 laser	Spectra-Physics	InSight X3
16x, 0.8 NA objective	Nikon	CFI75
4X, 0.28 NA objective	Olympus	XFLUOR